Optical and Quantum Electronics (2023) 55:178
https://doi.org/10.1007/s11082-022-04422-z

Influence of adsorption of gold and silver nanoclusters on structural, electronic, and nonlinear optical properties of pentacene-5,12-dione: a DFT study

Shradha Lakhera[1] · Meenakshi Rana[1] · Kamal Devlal[1]

Received: 16 August 2022 / Accepted: 21 November 2022

Abstract
The present study deals with the investigation of the change in the hyperpolarizability of Pentacene-2,5-dione (PD) on the introduction of the gold (Au) and silver (Ag) nanoclusters using the density functional theory (DFT). The involvement of the nanoclusters induces the intramolecular interactions, which is confirmed by the electrostatic potential plot and Mulliken charge distribution. The process of adsorption of metal clusters on the surface of PD is investigated by absorption spectra and the Raman spectra analysis. The global reactivity parameters validate a hike in the reactivity of the PD after the adsorption of Ag_3 and Au_3 nanoclusters. The study reported extraordinary enhancement in the hyperpolarizability of the metal nanoclusters adsorbed complexes. The high value of hyperpolarizability for PD-Ag_3 (184.22×10^{-30}esu) and PD-Au_3 (2057.26×10^{-30}esu) validates their applications in highly efficient NLO devices. The statistical calculation of radiative lifetime and light-harvesting efficiency reveals that probe PD can fruitfully contribute to the development of photo luminescent material and photosensitizer dye in dye-synthesized solar cells.

Keywords Nanoclusters · Density functional theory · Nonlinear optics · Pentacene-2,5-dione · Luminescent material · Dye-synthesized solar cells

1 Introduction

Aromatic hydrocarbon is a well-known category of reactive compounds having sigma bonds and delocalized π electrons between the carbon atoms (Omidi and Dadsetani 2016). These consist of multiple benzene rings clubbed together forming polycyclic hydrocarbons. Such molecules have considerable interest among theoretical and experimental researchers due to their versatile structure and high reactivity. Many studies have been reported to work on nonlinear optical (NLO) activity of different classes of aromatic hydrocarbons like anthracenes (Yanxin et al. 2021), quinacridone (Khan et al. 2019), naphthalene (Alyar 2013), pyrene (Khan et al. 2022), benzopyrenes (Jayakrishnan et al. 2016),

✉ Meenakshi Rana
mrana@uou.ac.in

[1] Department of Physics, School of Sciences, Uttarakhand Open University, Haldwani, Uttarakhand 263139, India

benzo-anthracene (Gott 1971), ovalene (Aryanpour et al. 2014), triphenylene (Gowda et al. 2019), chrysene (Tsague et al. 2022) and many more. The mentioned studies, thus, account for the high chemical reactivity of polycyclic hydrocarbons. Pentacene, on the other hand, is one of the classes of polycyclic aromatic hydrocarbons consisting of five linearly clubbed benzene rings (Chou and Cheng 2004). Pentacene and its derivatives have a number of applications in the development of organic thin-film transistors, organic NLO materials, solar cells, organic light-emitting diodes (OLEDs), etc. (Lee et al. 2003). Many studies have presented wide usage of Pentacene in the field of photovoltaics (Sadowski 2012; Srivastava and Tripathi 2022). Due to having high mobility, the derivatives of Pentacene are also used as p-type organic semiconductors (Kymissis et al. 2002). All the reported studies account for the high reactivity and applicability of the Pentacene and its derivatives in different branches of physical science. The major use of Pentacene and its derivatives was seen in the growth of the thin films (Ruiz et al. 2004). A study on Pentacene based radio frequency circuits has been reported (Baude et al. 2003). Pentacene and its compounds were also found to be used in the development of organic metal oxide semiconductor field-effect transistors (Kitamura and Arakawa 2008).

However, the adsorption of the organic compounds over the metal clusters has been of considerable interest to the researcher's community as the introduction of the metal nanoclusters has reportedly given immense enhancement to the electro-optical and chemical properties of the organic compounds (Amy et al. 2005). Atomic or molecular doping is also streaming field of material science that had led to advancement in technology (Tahmasebi et al. 2016; Zhu and Zhao 2022; Zhang et al. 2021; Li et al. 2022). Moreover, adsorbed and doped materials are proven more favourable in energy generating and storage applications like batteries and solar cells applications (Zhao et al. 2021; Wu et al. 2021; Tong et al. 2016; Mu et al. 2021; Zhang et al. 2022). Various studies have been reported for Pentacene from time to time. One such study targeting the enhanced hyperpolarizability of the Quinacridone after the adsorption of gold and silver nanoclusters has been reported and the results were highly appreciable (Felscia et al. 2018a). The study based on the adsorption studies of benzene, aniline and naphthylamine on reduced graphene oxides was also reported using experiments and theoretical density functional theory (DFT) (Yu et al. 2016). The development of photovoltaic cells with Pentacene adsorbed with fullerene (C_{60}) had been reported to improve the power efficiency of the cell by enhancing the short circuit current density (Pan and Rothberg 2007). The bonding between the gold and carbon atoms of Pentacene has been established using DFT and shed their applications in the second-order NLO applications (Yang et al. 2007). Studies with the substitution of gold atoms to Pentacene making complex $Au_2C_{22}H_{14}$ have also been reported to present the NLO responses of the complexes (Sun et al. 2009). NLO materials from alkali metal doped boron nitride cages are designed by many researchers (Maria et al. 2016, 2017; Munsif et al. 2018; Maria and Iqbal 2016a).

Thus, literature has a feast of kinds of studies reporting the NLO activity of Pentacene complexes with other metal atoms or clusters. One such derivative of pentacene namely Pentacene-2,5-dione (PD) has been considered for the present study. The study aims to establish the intensified NLO activity of the PD molecule after the adsorption of the silver (Ag_3) and gold (Au_3) metal nanoclusters. As the initial nucleation stage of silver and gold nanoparticle is the formation of the trimers (Ag_3 and Au_3) (Felscia and Rajkumar 2018; Felscia et al. 2019a) and numerous researches reporting adsorption studies of Ag_3 nanocluster has been accounted in the literature with tremendous rise in the NLO activities (Otaibi et al. 2022; Shakerzadeh et al. 2022). Thus, it is considered for the present study as the nanocluster. The chemical reactivity of the probe PD, PD-Ag_3, and PD-Au_3 complexes was established by molecular electrostatic

potential (MEP) surface and frontier molecular orbital (FMO) parameters. Vibrational spectra also presented the adsorption site of the nanoclusters over the surface of the PD molecule and highlights the description of the adsorption. The intramolecular charge transfer (ICT) was also identified between the metal nanocluster and the PD molecule.

2 Computational methods

Hartree–Fock is an ab-initio method with good accuracy in calculating nonlinear optical response. However, all the "pure" functionals have a fraction of HF non-local exchange energy replacing a similar fraction from the DFT local exchange energy. DFT on the other hand is known to be less time taking and more precise. Thus, DFT was preferred for all the ground state and excited state quantum chemical calculations. The geometry optimization of probe PD, PD-Ag_3, and PD-Au_3 was performed using B3LYP/6-311-G(++d,p), and B3PW91/LANL2DZ (Los Alamos National Laboratory double zeta) level of theory in Gaussian 09 program (Frisch 2010). The B3LYP/6-311-G(++d,p) is large basis set used for the ground state and excited state calculations of organic compounds whereas B3PW91/LANL2DZ basis set is considered more accurate for quantum mechanical calculations of metal clusters and numerous studies have been reported to establish the metal-to-molecule interaction using the same pair of functions (Cramer and Truhlar 2009; Tekarli et al. 2009; Felscia et al. 2019b). All the calculations of the PD molecule are done with singlet state. The availability of the unpaired electrons imparts to the doublet state. For PD-Ag_3 and PD-Au_3, the calculations are done in doublet state. This might be due to the availability of the unpaired electrons in Ag and Au atoms. The ground state optimization were carried out till threshold values of maximum force as 0.00045, RMS force 0.0003, maximum displacement 0.0018 and RMS displacement 0.0012 without any additional information sets. For TD-SCF calculations, convergence on RMS density matrix was at 1.00×10^{-8}, convergence on maximum density matrix was at 1.00×10^{-6}. The basis set superposition error (BSSE) was computed for the PD-Ag_3 and PD-Au_3 by B3PW91/LANL2DZ with counterpoise=2 procedure (Boys and Bernardi 1970). The empirical dispersion term for the PD-Ag_3 and PD-Au_3 using "Dispersion energy=Grimme GD3" procedure for B3PW91/LANL2DZ set of functions for getting the better understanding of the interactions between the molecule and the nanoclusters (Grimme et al. 2010). The natural bond orbital (NBO) analysis was also performed for PD-Ag_3, and PD-Au_3 for the prediction of the intramolecular interactions (Weinhold and Landis 2005). The chemical reactivity of the probe PD, PD-Ag_3, and PD-Au_3 was established using MEP surface and global reactivity parameters. Different reactivity parameters like bandgap (ΔE), ionization potential (IP), electron affinity (EA), chemical potential (CP), electronegativity (χ), are calculated with the help of Koopman's equations given below (Gritsenko and Baerends 2009; Yadav et al. 2021; Ojo et al. 2020; Akinyele et al. 2022):

$$\Delta E = E_{LUMO} - E_{HOMO} \tag{1}$$

$$IP = -E_{HOMO} \tag{2}$$

$$EA = -E_{LUMO} \tag{3}$$

$$CP = \frac{E_{HOMO} + E_{LUMO}}{2} \tag{4}$$

$$\chi = \frac{(IP + EA)}{2}, \tag{5}$$

The vibrational spectra was computed for the identification of the adsorption site of metal nanoclusters on PD. The Raman intensity was calculated for high frequency modes using expression:

$$I = \frac{f\left(\nu_o - \nu_i\right)^4 \mathrm{S}_i}{\nu_i\left[1 - \exp\left(-\frac{hc\nu_i}{\mathrm{kT}}\right)\right]} \tag{6}$$

where I is Raman intensity of the vibrational mode, f is a constant with value 10^{-12}, ν_o has value 9398.5 cm^{-1}. ν_i and S_i is the vibrational wavenumber and Raman activity of selected mode respectively. h is Planck constant with value 4.1357×10^{-15} eV K^{-1}, c is speed of light having value 3×10^8 m/s, K is Boltzmann constant with value 8.6173×10^{-5} eV K^{-1}, and T is temperature 293.5 K.

The NLO activity of the probe and metal nanoclusters adsorbed complexes was developed by polar frequency calculations. The tensor components were obtained for computing total isotropic polarizability (α_{total}), and anisotropy of polarizability ($\Delta\alpha$) and first order hyperpolarizability (β_{total}) using finite field theory approach (Yadav et al. 2021). These parameters are computed using following expression:

$$\alpha_{total} = \frac{1}{2}\left(\alpha_{xx} + \alpha_{yy} + \alpha_{zz}\right) \tag{7}$$

$$\Delta\alpha = \frac{1}{\sqrt{2}}\left[\left(\alpha_{xx} - \alpha_{yy}\right)^2 + \left(\alpha_{yy} - \alpha_{zz}\right)^2 + \left(\alpha_{zz} - \alpha_{xx}\right)^2 + 6\alpha_{xz}^2 + 6\alpha_{xy}^2 + 6\alpha_{yz}^2\right]^{\frac{1}{2}} \tag{8}$$

$$\beta_{total} = \left[\left(\beta_{xxx} + \beta_{xyy} + \beta_{xzz}\right)^2 + \left(\beta_{yyy} + \beta_{yzz} + \beta_{yxx}\right)^2 + \left(\beta_{zzz} + \beta_{zxx} + \beta_{zyy}\right)^2\right]^{\frac{1}{2}} \tag{9}$$

where α_{xx}, α_{yy}, and, α_{zz} are the tensor components of polarizability and β_{xxx}, β_{yyy}, and β_{zzz} are the tensor components of hyperpolarizability.

3 Results and discussion

3.1 Structure and charge analysis

PD has planar geometry with C1 point group symmetry due to which the dipole moment vectors of the atoms cancel each other (Kirtman et al. 1998). The 2O and 1O attached to the opposite sides give rise to a low magnitude of the dipole moment of 0.0002 Debye for the PD molecule. After the adsorption of Ag_3 and Au_3 nanoclusters, a rise in the dipole moment of the adsorbed complexes was observed due to their unsymmetrical structures. The value of dipole moment for PD-Ag_3 and PD-Au_3 was observed as 8.71 Debye and 3.96

Debye respectively. The high value of dipole moment was probably due to the larger differences between electronegativities of the donor and acceptor moieties present in the complexes (Lakhera et al. 2021; Rana et al. 2016; Yang et al. 2022; Wu et al. 2022; Rana and Chowdhury 2017). The rise in the dipole moment shows the enhanced chemical reactivity of the adsorbed complexes. The parameters obtained after the structure optimization of the PD adsorbed with Ag_2, Ag_4, Au_2, and Au_4 better supported our selection of the trimer for the present study. The dipole moment for the optimized geometries of PD-Ag_2, PD-Ag_4, PD-Au_2, and PD-Au_4 were calculated as 2.17, 4.17, 3.7, and 2.5 Debye respectively. The values of the dipole moment were comparatively lower than the value of dipole moment of PD-Ag_3 and PD-Au_3. The optimized geometries of the probe PD, and PD after adsorption of Ag_3 and Au_3 nanoclusters are illustrated in Fig. 1. The calculated empirical dispersion value of PD-Ag_3 is -33.711 kcal/mol and the calculated empirical dispersion value of PD-Au_3 is -32.014 kcal/mol. The comparison of these energy shows the higher empirical correction was added to the PD-Ag_3 and PD-Au_3 was quite stable than former. To get the better validation of the interaction between the molecule and the nanocluster, the interaction energy was computed using the following expression (Gordon and Jensen 1996):

$$E_{int} = E_{complex} - \left(\Sigma E_{component}\right) \tag{10}$$

where E_{int} is the interaction energy between the PD and nanocluster (Ag_3 and Au_3), $E_{complex}$ is the energy of the complex PD-Ag_3 and PD-Au_3, $E_{component}$ is the energy of the components of complex (say PD and Ag_3, $Au_{3)}$. The computed values of interaction energies of PD-Ag_3 and PD-Au_3 are − 13.74 kcal/mol and − 18.19 kcal/mol respectively. The more negative interaction energy is corresponding to the more stable complex. That means PD-Au_3 is higher than PD-$Ag_{3.}$ The BSSE energy of PD-Ag_3 was 0.00261 kcal/mol and PD-Au_3 was 0.00372 kcal/mol. The bond lengths of the PD, PD-Ag_3, and PD-Au_3 are mentioned in SD 1. The bond length of 1O=13C and 2O=14C of the carbonyl group in PD has lower bond lengths than the C=C bonds associated with the PD molecule. The C–H bonds have lower bond lengths showing the stability of the C–H bonds. The shorter the bond length, the lower will be the chances of bond dissociation, and the longer the bond, the higher will be the chances of easy dissociating of the bond (Lakhera et al. 2022a). The bond dissociation will give rise to the charge cloud resulting in ICT. Similarly, the bond angles (SD 2) had a large variation in magnitudes between the C–H bonds and C=O bonds. High magnitudes of the bond angles lead to easier bond dissociation. After the adsorption of the metal clusters on the surface of the PD molecule, there seems a rise in the bond length of the C=O bonds of the carbonyl group. The larger bond are weaker and need less energy to dissociate and thus, they can easily be dissociated with very low amount of energy. This shows the inverse proportionality of bond length with the stability of the bond. Or it can be considered that the bonds between the nanoclusters i.e., Au and Ag atoms in their respective nanoclusters are bonded with larger bonds. Thus, the bonds will get easily dissociated and give free electron pairs. This highlights the participation of nanoclusters in inducing the intramolecular interactions (Rana et al. 2017). The optimization parameters suggest that there is a possibility of ICT between the PD and the metal nanoclusters and validates the enhancement of electrostatic interaction after the adsorption of metal nanoclusters on the surface of PD. The Mulliken charge distribution of the optimized geometries of the PD, PD-Ag_3, and PD-Au_3 are illustrated in Fig. 1. The color bar at the top of the Fig. 1 indicates the positive and negative charge of the atoms. The red color indicates the negative charge and the green color indicates the positive charges of the atoms (Rana et al. 2018). The atoms of the optimized geometries were indicated by the charge

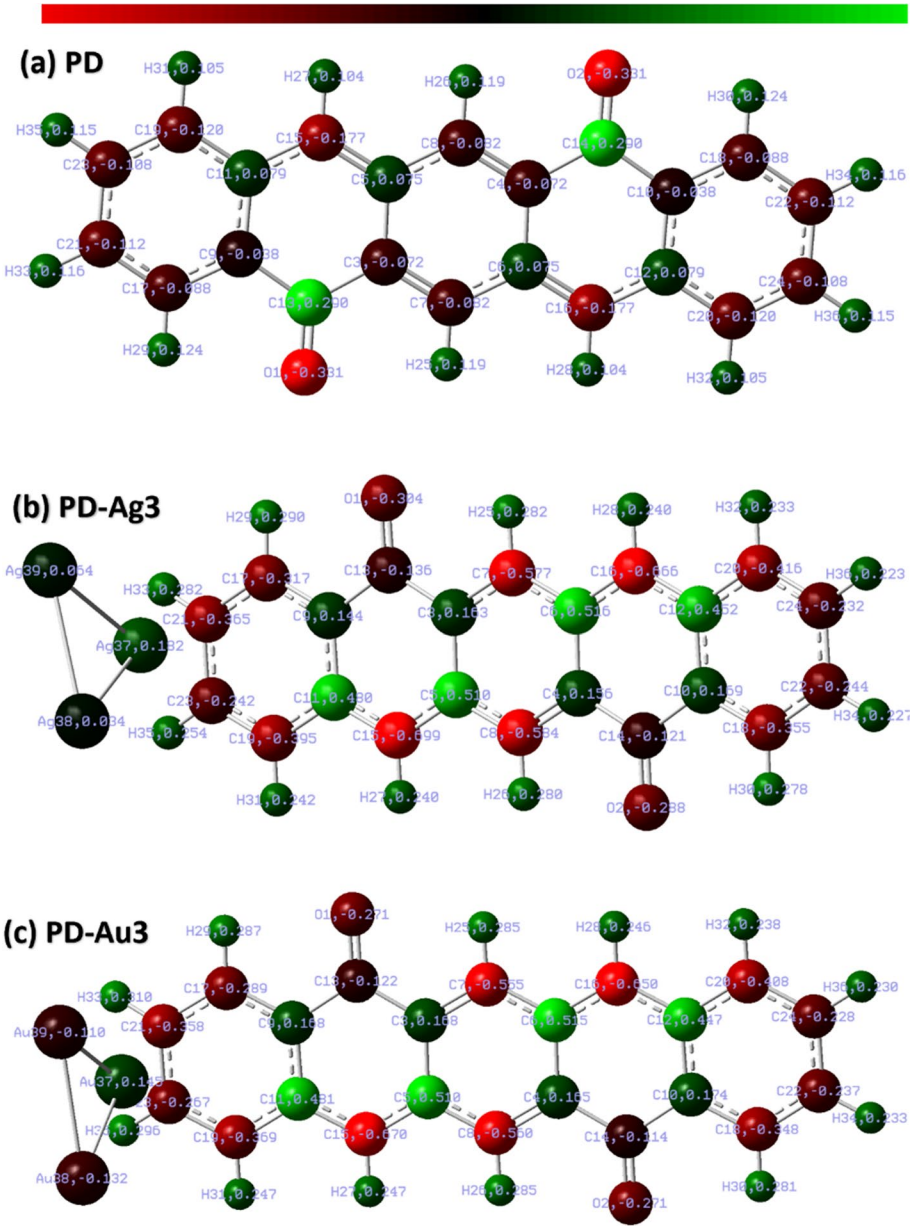

Fig. 1 Optimized geometries of PD, PD-Ag_3 and PD-Au_3 at B3PW91/LANL2DZ set of functions illustrating the Mulliken charge distribution

color code. The charge distribution of the PD distributed in the range ± 0.667 e shows the positive charge contribution of the hydrogen atoms of C–H bonds and the negative charge distribution of the oxygen atoms 1O and 2O (− 0.225 e each) of carbonyl groups. The variation between the charges of the hydrogen atoms and carbonyl groups expresses

the intramolecular interactions between these two parts of PD. After the introduction of Ag_3 and Au_3 nanoclusters, the involvement of the Ag and Au atoms in the intramolecular interactions was observed. The charge distribution of PD-Ag_3 and PD-Au_3 complex was distributed in ranges ± 0.669 e and ± 0.806 e respectively. The Ag atoms 37Ag (0.182 e), 38Ag (0.034 e), and 39Ag (0.064 e) contribute to the positive charge indicating the participation of the Ag_3 nanocluster as a donor moiety. The Au_3 atoms 37Au (0.154 e), 38Au (− 0.143 e), and 39Au (− 0.13 e) impart positive as well as negative to the overall charge distribution of the complex. The variation of the charges between the Au atoms and carbon and oxygen atoms of the carbonyl groups shows the intramolecular interactions between the Au_3 nanocluster and the carbonyl groups. Thus, the charge distribution highlights the enhanced intramolecular interactions in PD molecules after the adsorption of the Ag_3 and Au_3 nanoclusters.

3.2 MEP surface analysis

MEP surface is used to illustrate the ICT of molecules. These surfaces are used to locate the areas with electron excess and electron deficiency of the molecule which are responsible for inducing ICT within the molecule (Oyeneyin et al. 2022). There are five colors that a MEP surface constitutes and they are in a sequence from negative to positive nature as red < yellow < green < light blue < dark blue. The moieties over which the surface is of red color are highly negative or electronegative in nature whereas the dark blue surface indicates the positive or electropositive moieties. Green color indicates the neutral part of the molecule or the region that doesn't participate in the intramolecular interactions. Yellow is slightly electronegative whereas sky blue is slightly electropositive in nature. The moieties with donor properties are known as positive regions and are indicated by blue color while the acceptor moieties are called negative and are indicated by red color (Lakhera et al. 2022a). The potential range of the MEP surface is indicated by the color band at the top of

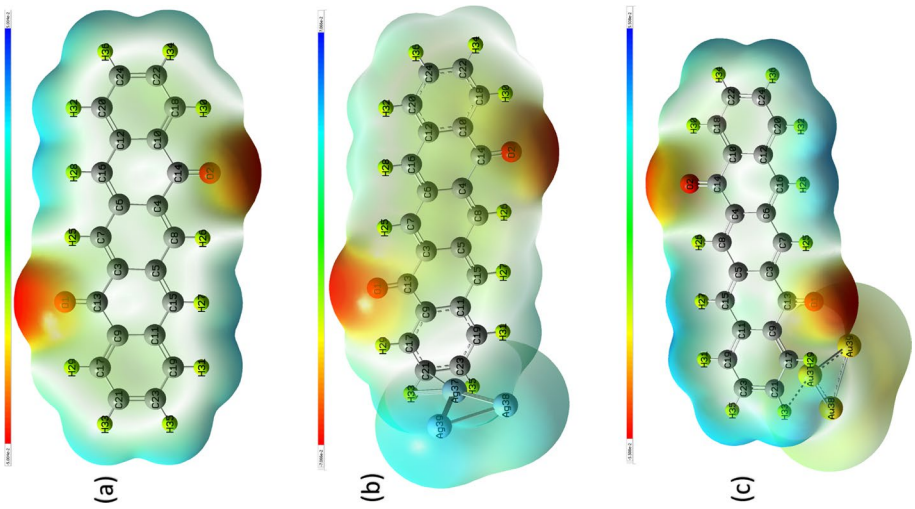

Fig. 2 MEP surface of PD, PD-Ag_3 and PD-Au_3 computed by B3PW91/LANL2DZ. Red color regions indicates the electronegative part and blue color indicates the electropositive part of the title molecules

the surface. The MEP surface of PD illustrated in Fig. 2a validates the positive nature of C–H bonds of the benzene rings and the negative nature of 1O=13C and 2O=14C bonds of the carbonyl group. The electrostatic potential range for probe PD is $\pm 5.004 \times 10^{-2}$ electrons/Å^3. The hydrogen atoms are highly electropositive and oxygen atoms are highly electronegative. The MEP map identifies the transportation of heavily accumulated charge from the C–H bonds towards the C=O bonds of the carbonyl groups. Adsorption of Ag and Au nanoclusters over the PD molecule induces a redistribution of electron density. The involvement of the Ag and Au nanoclusters in ICT within the PD-Ag_3 and PD-Au_3 complexes was identified by the MEP map of PD-Ag_3 and PD-Au_3 shown in Fig. 2b, c respectively. It is observed that the blue region over the C–H bonds of the PD molecule is shifted over the Ag_3 nanocluster after the adsorption of the Ag_3 nanocluster. Thus, the Ag_3 nanocluster acts as a donor part of the PD-Ag_3 complex, and ICT is seen to act from Ag_3 towards the carbonyl groups. This supports the results analyzed from Mulliken charge variation. A similar kind of ICT is seen in the PD-Au_3 complex where the charge cloud dislocated from the Au_3 nanocluster to carbonyl groups. The availability of the donor and acceptor moieties within the PD, PD-Ag_3, and PD-Au_3 validates the enhanced ICT within the PD molecule after the introduction of the Ag_3 and Au_3 metal nanoclusters. This shows the high chemical reactivity of PD, PD-Ag_3, and PD-Au_3 as mentioned by structural parameters.

3.3 Natural bond orbital (NBO) analysis

NBO analyses were performed to describe the intramolecular/intermolecular electronic interactions (Lakhera et al. 2022b). The charge delocalization of donor NBO towards acceptor NBO give rise to the higher degree of conjugation leading to the stability of the complex. The second order perturbation approach was used for computing the stabilization energy ($E(2)$) corresponding to each donor (i) and acceptor (j) atom. The $E(2)$ corresponding to the delocalization of each i → j were calculated using the expression:

$$E(2) = \Delta E_{ij} - q_i \left(\frac{f_{ij}^2}{E_j - E_i} \right) \tag{11}$$

where $F(i,j)$ are the Fock matrix element between i and j NBO orbitals, E_j and E_i are the energies of the acceptor and donor NBOs. The interactions with higher values of $E(2)$for PD-Ag_3 and PD-Au_3 are listed in Table 1. In case of PD-Ag_3, second order perturbation theory analysis of NBO, higher values of $E(2)$ were obtained for interactions of 37Ag with the atoms of PD molecule. This shows the participation of atom 37Ag in charge dislocation. The maximum value of stabilization energy was observed for the interaction between 21C and 37Ag. On the other hand, the interaction between the 21C and 37Au has the maximum value of stabilization energy of 6.74 kcal/mol for PD-Au_3. Thus, higher value of stabilization was observed for PD-Au_3 which shows the higher intramolecular charge transfer between donor and acceptor moieties of PD-Au_3 as compared to PD-Ag_3.

3.4 Molecular orbital analysis

The FMO parameters are derived from the energies corresponding to the highest occupied and lowest unoccupied molecular orbitals (HOMO–LUMO). These parameters are computed to confirm the chemical reactivity of the molecules (Rana et al. 2017). All the computed FMO parameters are listed in Table 2. The energy gap or band gap (ΔE) is the virtue

Table 1 Second order perturbation theory analysis of Fock matrix in NBO basis of PD-Ag_3 and PD-Au_3

S. no.	Donor NBO (*i*)	Acceptor NBO (*j*)	*E*(2) (kcal/mol)	*E*(*j*)–*E*(*i*) (au)	*F*(*i*,*j*) (au)
PD-Ag_3					
1	σ (C_{17}–C_{21})	LP* (Ag37)	1.14	0.82	0.039
2	π (C_{19}–C_{23})	LP* (Ag37)	1.27	0.39	0.03
3	σ (C21–C23)	LP* (Ag37)	1.7	0.81	0.047
4	σ (C21–C33)	LP* (Ag37)	1.13	0.64	0.034
5	CR (C21)	LP* (Ag37)	1.20	10.18	0.142
6	LP (C21)	LP* (Ag37)	6.11	0.16	0.041
7	LP (C21)	LP* (Ag37)	1.96	0.24	0.034
8	LP (C21)	LP* (Ag37)	3.49	0.28	0.051
9	LP* (Ag37)	RY* (C21)	2.56	0.59	0.082
10	LP* (Ag37)	σ* (C19–C23)	1.86	0.02	0.012
PD-Au_3					
1	σ (C17–C21)	LP*(Au37)	1.07	0.88	0.04
2	σ (C19–C23)	LP*(Au37)	3.00	0.46	0.051
3	σ (C19–C23)	σ*(Au37–Au38)	1.36	0.36	0.03
4	σ (C21–C23)	LP*(Au37)	3.06	0.89	0.067
5	σ (C21–C33)	LP*(Au37)	1.55	0.72	0.043
6	σ (C23–C35)	LP*(Au37)	1.25	0.72	0.039
7	CR (C21)	LP*(Au37)	1.59	10.26	0.166
8	CR (C23)	LP*(Au37)	1.34	10.27	0.152
9	LP (C21)	LP(Au37)	6.74	0.36	0.081
10	LP (C21)	σ*(Au37–Au39)	3.84	0.24	0.051
11	σ*(C19–C23)	σ*(Au37–Au38)	1.33	0.07	0.026
13	CR (Au37)	σ*(C19–C23)	1.15	4.11	0.095

Table 2 Frontier molecular orbital parameters for the PD, PD-Ag_3 and PD-Au_3 molecule

S. no.	Molecular property	PD	PD-Ag_3	PD-Au_3
1	E_{HOMO}	−5.75	−5.23	−4.91
2	E_{LUMO}	−3.61	−3.22	−3.89
3	Energy gap (Δ*E*)	2.14	2.01	1.02
4	Ionization potential (*IP*)	5.75	5.23	4.91
5	Electron affinity (*EA*)	3.61	3.22	3.89
6	Chemical potential (*CP*)	−4.68	−4.22	−4.4
7	Electronegativity (χ)	4.68	4.22	4.4

All values are in eV

that accounts for how easily electrons from the HOMO can transit to LUMO. Molecules having lower values of Δ*E* shows high reactivity (Lakhera et al. 2022c). It is seen that the Δ*E* for probe PD was 2.14 eV but a decrease in the Δ*E* was observed when the metal nanoclusters are adsorbed by the PD molecule. Thus, the low value of Δ*E* for PD-Ag_3 (2.01 eV) and PD-Au_3 (1.02 eV) shows that the electrons of PD can easily jump up to the higher energy state when combined with metal nanoclusters. However, the value of

ΔE for PD-Au_3 is lower than that of PD-Ag_3. The lower bandgap has a greater probability of the free charge transiting to higher energy states. This shows that the PD-Au_3 might have larger absorbance than PD-Ag_3. The ionization potential (*IP*) of a molecule should be low to remove the electrons easily from the outermost shell of the donor atoms. PD-Au_3 (4.91 eV) has the lowest value of *IP* than the probe PD (5.75 eV) and PD-Ag_3 (5.23 eV). The high value of electron affinity (*EA*) shows the greater tendency of the atoms to gain electrons. The *EA* is highest for PD-Au_3 (3.89 eV). The chemical potential (*CP*) shows the high tendency of the molecules to undergo charge transfer and molecules having a high value of *CP* are highly reactive. PD, PD-Ag_3 and PD-Au_3 have the value of *CP* mutually close showing the high chemical reactivity of the three title molecules. The high value of electronegativity (χ) for PD-Ag_3 as compared to PD-Ag_3 shows how easily Au_3 adsorbed complex attracts the shared electrons. The distribution of the HOMO–LUMO surface over the title molecules is illustrated in Fig. 3a–c. The red surface indicates the positive and the green surface indicates the negative phases in molecular orbital wave function. The HOMO–LUMO surface is uniformly distributed over the geometry of PD. Larger positive and negative surfaces over the metal nanoclusters in HOMO are shifted over the benzene rings in LUMO. This shifting of surfaces shows that ICT exists from nanoclusters to PD molecules as stated by structural analysis. The chemical reactivity of PD undergoes enhancement as the Ag_3 and Au_3 metal nanoclusters get adsorbed to the surface of the PD molecule. Thus, the analysis of the FMO parameters shows that the introduction of Ag_3 and Au_3 nanoclusters to PD intensifies its chemical reactivity.

3.5 Absorption analysis

The absorption spectra for PD, PD-Ag_3, PD-Au_3 compounds are illustrated in Fig. 4 and the details of the transitions had been listed in SD 3. The transition $S_0 \rightarrow S_1$ of PD occurred at wavelength 561 nm was majorly responsible for the broad absorption band of PD. The oscillator strength (*f*) for this transition was observed as 0.719 and the excitation energy for this mode was computed as 2.2 eV. The high value of excitation energy and the *f* reveals the high reactivity of the PD. It was observed that the introduction of metal nanoclusters to the PD shows a rise in the intensity of the transitions and bathochromic shift of wavelength. Broad spectra for PD-Ag_3 and PD-Au_3 were seen to range between 500 and 3000 nm. The transition $S_0 \rightarrow S_6$ for PD-Ag_3 and PD-Au_3 occurred at wavelengths of 662 and 637 nm

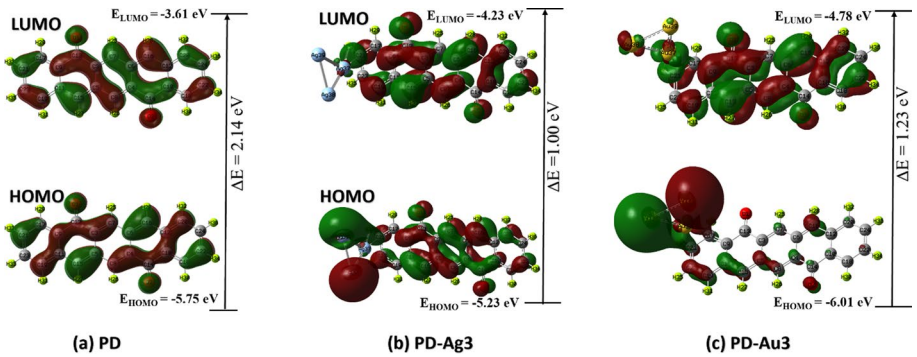

Fig. 3 Molecular orbitals for the **a** PD, **b** PD-Ag_3 and **c** PD-Au_3. The lower structure shows HOMO and upper structure shows LUMO of the respective molecules and the band gap is represented by ΔE

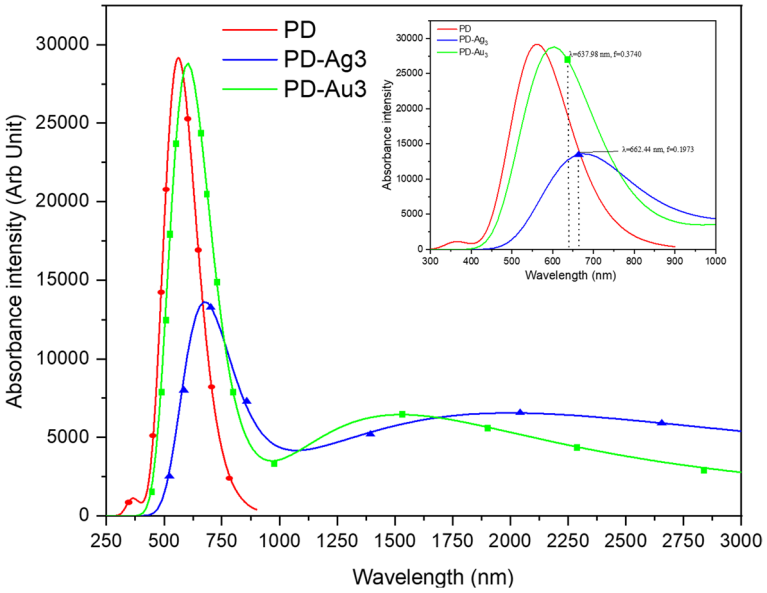

Fig. 4 Absorption spectra of PD, PD-Ag_3 and PD-Au_3 computed using B3PW91/LANL2DZ basis set. Insight of Fig. 4 indicates the crucial peaks of PD-Ag_3 and PD-Au_3 with their wavelength and oscillator strength

respectively were the crucial transition (transitions having the highest oscillator strength) for both of spectra. Higher values of oscillator strength indicate a higher possibility of the transition occurring. Therefore, it can be considered that the transition in PD-Au_3 is most likely to occur than in PD-Ag_3. Moreover, the rise in the intensity of the absorption in PD-Au_3 also indicates the involvement of the nanocluster in the ICT. This creates a close relationship between the ICT developed by the HOMO–LUMO surface distribution in the molecular orbital analysis (Li et al. 2020; Hou et al. 2014; Chen et al. 2005). As the HOMO densities plot indicates the availability of excess electrons in PD-Au_3, it can be said that PD-Au_3 possesses more possibility of undergoing ICT between PD and Au_3. The absorbance shifts in the wavelength and intensity were mainly due to the interference in the hyperconjugation of the bonds. This leads to the rise in the count of partial double bonds (π bonds) giving rise to lone pair of electrons. Thus, the hyperconjugation in the metal clusters results in absorbance shifts. Moreover, the rise in conjugation is proportional to the bond lengths. This also makes a good agreement with the higher bond lengths obtained for the metal clusters in structural analysis. The higher absorbance intensity was also in accord with band gap of the complex.

3.6 Vibrational analysis

The nature of adsorption of metal nanoclusters on the surface of the PD molecule was established by computing vibrational spectra using the B3PW91/LANL2DZ basis set. The important vibrational modes and the assignments are illustrated in Fig. 5 and listed in SD 3. We have observed a rise in the intensities of different vibrational modes after the introduction of the metal nanoclusters. This rise seems to confirm the enhancement of the

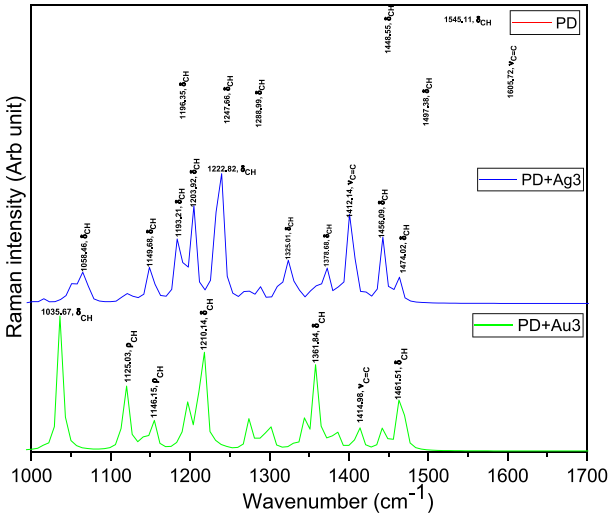

Fig. 5 Vibrational spectra for the PD, PD-Ag_3 and PD-Au_3 molecule computed using B3PW91/LANL2DZ basis set (Symmetric stretching-ν, torsional bending in plane (scissoring)-δ, twisting-τ, rocking-ρ, and wagging-ω, stretching of C–C bonds in benzene- λ)

Table 3 Computed values of α_{total}, $\Delta\alpha$ and β_{total} for the PD, PD-Ag_3, and PD-Au_3 molecule

Molecule	α_{total} (esu)	$\Delta\alpha$ (esu)	β_{total} (esu)
PD	54.73×10^{-24}	211.76×10^{-24}	0.000181×10^{-30}
PD-Ag_3	129.79×10^{-24}	532.44×10^{-24}	184.22×10^{-30}
PD-Au_3	108.65×10^{-24}	436.42×10^{-24}	2057.26×10^{-30}

chemical reactivity of the PD after adsorption of the metal nanoclusters. The low frequency modes for the vibration of metal nanoclusters (113.8 cm^{-1} for PD-Ag_3 and 113.8 cm^{-1} and 160.56 cm^{-1} for PD-Au_3) were observed showing adsorption interaction between the PD and metal nanoclusters. The out of plane bending of the geometry of PD was observed at 541.8, 549.94, 620.81, and 698.17 cm^{-1}. Contrastingly, the out of plane vibrations for PD-Ag_3 are observed at comparatively higher frequencies 556.9, 628.86, 697.36, 740.99, and 793.26 cm^{-1}. Similar rise in the frequency was observed for the out of plane vibrational modes for PD-Au_3 at 535.59, 548.85, 629.21, 696.78, 739.27, 778.67 cm^{-1}. The carbonyl groups of the PD show ν_{CO} mode at 1695.05 cm^{-1}. The ν_{CO} mode for PD-Ag_3 and PD-Au_3 was identified at 1586.11 cm^{-1} and 1584.77 cm^{-1} respectively. Stretching of C=C bond of benzene ring for PD-Ag_3 (1412.14 cm^{-1}, and 1418.92 cm^{-1}) and PD-Au_3 (1414.98 cm^{-1}, and 1427.09 cm^{-1}) confirms the potential site for adsorption in each case.

3.7 NLO analysis

NLO materials interacting with electric field lines must have a high polarization density. When a material is kept in the homogeneous electric field, the energy possessed by the material is expanded as Taylor's series expansion where the α and β are the coefficients of the Taylor series expansion (Hutchings et al. 1992). These coefficients are correlated to NLO activity as the high value of the coefficient of high order derivatives leads to high NLO activity of the molecule. Thus, to predict the NLO activity, α_{total}, $\Delta\alpha$ and β_{total} are computed for the title molecules. All the computed tensor components of the α_{total}, $\Delta\alpha$ and

β_{total} for PD, PD-Ag_3, and PD-Au_3 molecules are mentioned in SD 3, and SD 4 respectively and the values of polarizability parameters are mentioned in Table 3. The value of α_{total} is computed as 54.73×10^{-24}esu for probe PD molecule but after the adsorption of Ag_3 and Au_3 nanoclusters, this value was increased to 129.79×10^{-24} and 108.65×10^{-24}esu respectively. These values are approximately twice the value of α_{total} for probe PD molecule. The values of $\Delta\alpha$ for PD-Ag_3 (532.44×10^{-24}esu) and PD-Au_3 (436.42×10^{-24}esu) are higher than the $\Delta\alpha$ for PD (211.76×10^{-24}esu). A very low value of β_{total} for probe PD (0.000181×10^{-30} esu) was computed but an extraordinary rise in the values of the β_{total} was observed after the adsorption of metal nanoclusters. The values of β_{total} for PD-Ag_3 and PD-Au_3 were observed as 184.22×10^{-30}esu and 2057.26×10^{-30}esu. These values are 10,117,790 and 11,427,777 times higher than the β_{total} for probe PD. Two-level mode was also used for the validation of the NLO activity of complex. The dependency of hyperpolarizability on the dominating factors was examined by the two-level mode by using expression of hyperpolarizability (Maria and Iqbal 2016b):

$$\beta_{total} = \frac{\Delta\mu \times f}{(\Delta E)^3} \tag{12}$$

where Δμ is the difference between the dipole moment of ground state and crucial excited state, f is the oscillator strength of the crucial transition obtained in UV–Vis spectra. Crucial transition is the transition having the higher value of oscillator strength. ΔE is the excitation energy of the crucial transition. For both PD-Ag_3 and PD-Au_3, $S_0 \rightarrow S_6$ was the crucial transition with f values equal to 0.1973 and 0.374 respectively. According to two-level mode, the hyperpolarizability shares the direct proportionality to the f values, in our case f was larger for PD-Au_3. Thus, PD-Au_3 was verified to have higher value of β_{total} and hence high NLO activity. Validation of the findings was done by comparing the β_{total} of PD-Ag_2, PD-Ag_4, PD-Au_2, and PD-Au_4 with that of PD-Ag_3 and PD-Au_3. The values of β_{total} of PD-Ag_2, and PD-Ag_4 were 481.57×10^{-30}esu, and 149.36×10^{-30}esu respectively. PD-Ag_3 has higher β_{total} than PD-Ag_4 but less than that of PD-Ag_2. In case of Au nanoclusters, the values of β_{total} for PD-Au_2, and PD-Au_4 were 10.66×10^{-30}esu, and 59.72×10^{-30}esu respectively which are comparatively much lower than the PD-Au_3. This shows that PD give promising NLO activity when adsorbed with the Au trimer. The value of β_{total} for pure Ag_3 and Au_3 clusters were computed as 0.8×10^{-30}esu, and 73.77×10^{-30}esu respectively. There are some studies in the literature that had reported high NLO activity of the pure nanoclusters. But pure Ag_3 and Au_3 clusters have significantly lower NLO responses. In comparison with the generally used reference NLO material Urea (0.781×10^{-30}esu), the value of β_{total} for PD-Ag_3 and PD-Au_3 are 236 and 2637 times higher (Cassidy et al. 1979). Thus, this comparison is fairly enough to justify that the PD can act as an excellent NLO material when adsorbed with Ag_3 and Au_3 nanoclusters (Fig. 6).

3.8 Radiative and light harvesting properties

The absorption spectra were computed for the probe PD molecule to get an idea about the electronic transitions. The spectra comprised of a broad strong absorption band identified with its peak at 361 nm wavelength. The transition $S_0 \rightarrow S_1$ occurred at the peak wavelength with f of 0.719 and excitation energy 2.20 eV. The other two transitions $S_0 \rightarrow S_2$ and $S_0 \rightarrow S_3$ occurred at wavelengths 246 and 246 nm respectively. The high excitation energy highlights the possibility of the $\pi \rightarrow \pi^*$ and $n \rightarrow \pi^*$ nature of the $S_0 \rightarrow S_1$ transition. Thus, the existence of such transitions shows the ICT in the PD

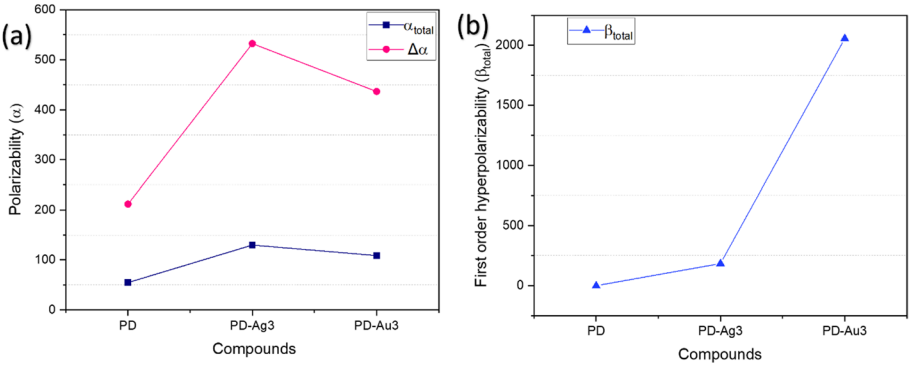

Fig. 6 Comparative plots of (a) polarizability (α_{total} and $\Delta\alpha$) and (b) β_{total} for the PD, PD-Ag_3, and PD-Au_3 molecule illustrating the high value of polarizability parameters for PD after adsorbing Ag_3 and Au_3 nanoclusters

molecule. The absorption spectra of PD was also used to establish the radiative and light-harvesting property of the probe molecule. The radiative lifetime (τ) was computed by below given formula (Felscia et al. 2018b):

$$\tau = \frac{c^3}{2fE^2} \tag{13}$$

where c is the speed of light and f and E are the oscillator strength and the excitation energy obtained in the absorption spectra respectively. The radiative lifetime accounts for the nature of transitions possessed by the molecules i.e., whether the molecules emit radiation during the transitions or the transitions are non-radiative. The former is called emissive transition and the latter is called non-emissive transition. However, the transitions having lifetime values larger than 10 are non-radiative. The electronic transitions for which the τ value is less than 10 are known to be radiative and these transitions eject energy in the form of photons (Poor and Flores 2014). Thus, for the PD molecule, the value of τ is computed to be 5.9 nm ~ 6 nm. The $\tau < 10$ for PD indicates that the transition $S_0 \rightarrow S_1$ occurred between the HOMO–LUMO of PD was radiative and shows its nature to possess photoluminescence (Bünzli et al. 2010). Thus, this establishes the potent applicability of PD molecules as an active luminescent material.

f is also used for calculating the light harvesting efficiency (LHE) for PD using the below mentioned formula (Lakhera et al. 2022d):

$$\text{LHE} = 1 - 10^{-f} \tag{14}$$

LHE measures the efficiency of any material to increase the ability of any solar cell to convert light energy into electrical energy. Thus, the applicability of the molecule to be used as photosensitizer dye in Dye-Sensitizer Solar Cells (DSSC) is statistically explained by LHE (Mary et al. 2019). For PD, the LHE is computed to be 80.91. The adsorption of Ag_3 and Au_3 on the PD, gave a decrease in the LHE of the compounds PD-Ag_3 (27%) and PD-Au_3 (20%). This can be due to the reflective nature of the Ag and Au. These materials do not absorb light up to the extent that is required for solar cells, and therefore give a lustrous glare. Thus, PD can convert 80% of the light incident on it into electrical energy. Hence, PD synthesized dye can lead to tremendous enhancement of the efficiency of solar cells.

4 Conclusion

A complete study of quantum mechanical properties of PD in probe state and adsorbed with Ag_3 and Au_3 nanoclusters were reported in the paper. The adsorption sites of the nanoclusters were identified by the high Raman intensity modes in vibrational spectra. The PD was found highly chemically reactive right after the adsorption of the Ag_3 and Au_3 nanoclusters and their chemical reactivity was verified using FMO parameters. The MEP surface over the nanoclusters also validated the electropositive character of nanoclusters and established their participation in inducing the ICT within the complex structures. In particular, the DFT calculations indicate the tremendous rise in the NLO activity of the PD after the adsorption of the Ag_3 and Au_3 nanoclusters. Thus, it can be concluded that the studied complexes hold considerable NLO activity and can be recommended for the high-tech applications of efficient NLO materials. Also, the experimental design of the studied complexes will be surely generative. The low value of τ signifies the radiative emission of photons resulting in the application of PD as a potent photoluminescent molecule. Employment of PD as a photosensitizer dye was noted by its high LHE. Thus, the probe PD can better act as a photoluminescent material as well as a dye in DSSC.

Supplementary Information The online version contains supplementary material available at https://doi.org/10.1007/s11082-022-04422-z.

Author contributions SL: Data curation, Writing-Original draft preparation, Visualization, Investigation, Software, Validation. MR: Conceptualization, Methodology, Writing-Reviewing and Editing, Supervision. KD: Conceptualization, Writing-Reviewing and Editing.

Funding The authors declare that this research received no specific grant from any funding agency.

Availability of data and materials Structure: https://pubchem.ncbi.nlm.nih.gov/. Extension conversion: http://openbabel.org/wiki/Main_Page. Optimization: https://gaussian.com/. Data analysis: https://gaussian.com/gaussview6/. Graph plotting: https://www.originlab.com/.

Declarations

Competing interests The authors declare that they have no known competing financial interests or personal relationships that could have appeared to influence the work reported in this paper.

Ethical approval I give my consent for the publication of identifiable details, which include data and pictures to be published in the Journal "Optics and Quantum Electronics"**.**

References

Akinyele, O.F., Adekunle, A.S., Olayanju, D.S., Oyeneyin, O.E., Durodola, S.S., Ojo, N.D., Aanuoluwapo, A.A., Ajayeoba, T.A., Olasunkanmi, L.O.: Synthesis and corrosion inhibition studies of (E)-3-(2-(4-chloro-2-nitrophenyl)diazenyl)-1-nitrosonaphthalen-2-ol on Mild Steel dissolution in 0.5 M HCl Solution—experimental, DFT and Monte Carlo Simulations. J. Mol. Struct. **1268**, 133738 (2022). https://doi.org/10.1016/j.molstruc.2022.133738

Alyar, H.: A review on nonlinear optical properties of donor–acceptor derivatives of naphthalene and Azanapthelene. Rev. Adv. Mater. Sci. **34**, 79–87 (2013)

Amy, F., Chan, C., Kahn, A.: Polarization at the gold/pentacene interface. Org. Electron. **6**(2), 85–91 (2005). https://doi.org/10.1016/j.orgel.2005.03.003

Aryanpour, K., Shukla, A., Mazumdar, S.: Electron correlations and two-photon states in polycyclic aromatic hydrocarbon molecules: a peculiar role of geometry. J. Chem. Phys. **140**, 104301 (2014). https://doi.org/10.1063/1.4867363

Baude, P.F., Ender, D.A., Haase, M.A., Kelley, T.W., Muyres, D.V., Theiss, S.D.: Pentacene-based radio-frequency identification circuitry. Appl. Phys. Lett. **82**(3964), 3964 (2003). https://doi.org/10.1063/1.1579554

Boys, S.F., Bernardi, F.: The calculation of small molecular interactions by the differences of separate total energies: some procedures with reduced errors. Mol Phys. **19**, 553–556 (1970)

Bünzli, J.C.G., Chauvin, A.S., Kim, H.K., Deiters, E., Eliseeva, S.V.: Lanthanide luminescence efficiency in eight- and nine-coordinate complexes: role of the radiative lifetime. Coord. Chem. Rev. **254**(21–22), 2623–2633 (2010). https://doi.org/10.1016/j.ccr.2010.04.002

Cassidy, C., Halbout, J.M., Donaldson, W., Tang, C.L.: Nonlinear optical properties of urea. Opt. Commun. **29**(2), 243–246 (1979). https://doi.org/10.1016/0030-4018(79)90027-0

Chen, W., Li, Z.-R., Wu, Di., Li, R.-Y., Sun, C.-C.: Theoretical investigation of the large nonlinear optical properties of $(HCN)_n$ Clusters with Li Atom. J. Phys. Chem. B **109**(1), 601–608 (2005). https://doi.org/10.1021/jp0480394

Chou, W.Y., Cheng, H.L.: An orientation-controlled pentacene film aligned by photoaligned polyimide for organic thin-film transistor applications. Adv. Funct. Mater. **14**(8), 811–815 (2004). https://doi.org/10.1002/adfm.200305047

Cramer, C.J., Truhlar, D.G.: Density functional theory for transition metals and transition metal chemistry. Phys. Chem. Chem. Phys. **11**, 10757–10816 (2009). https://doi.org/10.1039/B907148B

Felscia, U.R., Rajkumar, B.J.M.: Computational study of quinacridone on silver and gold clusters: applications to organic light emitting diodes and nonlinear optical devices. Mater. Lett. (2018). https://doi.org/10.1016/j.matlet.2018.03.149

Felscia, R., Rajkumar, B.J.M., Mary, B.: Charge transport properties of pyrene and its derivatives: optoelectronic and nonlinear optical applications. J. Mater. Sci. **53**, 15213–15225 (2018a). https://doi.org/10.1007/s10853-018-2690-9

Felscia, U.R., Rajkumar, B.J.M., Mary, M.B.: Theoretical investigations on nonlinear fused 4-ring systems: Application to OLED and NLO devices. Synth. Met. **246**, 31–38 (2018b). https://doi.org/10.1016/j.synthmet.2018.09.008

Felscia, U.R., Rajkumar, B.J.M., Sankar, P., Philip, R., Briget Mary, M.: Theoretical and experimental investigations of nitropyrene on silver for nonlinear optical and metal ion sensing applications. Mater. Chem. Phys. (2019a). https://doi.org/10.1016/j.matchemphys.2019.122466

Felscia, U.R., Rajkumar, B.J.M., Sankar, P., Philip, R., Mary, M.B.: Theoretical and experimental investigations of nitropyrene on silver for nonlinear optical and metal ion sensing applications. Mater. Chem. Phys. (2019b). https://doi.org/10.1016/j.matchemphys.2019.122466

Frisch, M.J.: Gaussian 09, Revision B.01. Gaussian Inc., Wallingford CT (2010)

Gordon, M.S., Jensen, J.H.: Understanding the hydrogen bond using quantum chemistry. Acc. Chem. Res. **29**, 536–543 (1996). https://doi.org/10.1021/ar9600594

Gott, J.R.: Effect of molecular structure on optical second-harmonic generation from organic crystals. J. Phys. B at. Mol. Phys. **4**, 116 (1971)

Gowda, A., Jacob, L., Patra, A., George, A., Philip, R., Kumar, S.: Synthesis, mesomorphic properties and nonlinear optical studies of alkyl and alkoxy phenylacetylene containing phenazine fused extended triphenylene discotic liquid crystalline dyes. Dyes Pigments **160**, 128–135 (2019). https://doi.org/10.1016/j.dyepig.2018.07.052

Grimme, S., Antony, J., Ehrlich, S., Krieg, H.: A consistent and accurate ab initio parameterization of density functional dispersion correction (DFT-D) for the 94 elements H-Pu. J. Chem. Phys. **132**, 154104 (2010). https://doi.org/10.1063/1.3382344

Gritsenko, O., Baerends, E.J.: The analog of Koopmans' theorem for virtual Kohn-Sham orbital energies. Can. J. Chem. (2009). https://doi.org/10.1139/V09-088

Hou, Na., Wu, Di., Li, Y., Li, Z.-R.: Lower the Electron affinity by halogenation: an unusual strategy to design superalkali cations. J. Am. Chem. Soc. **136**(7), 2921–2927 (2014). https://doi.org/10.1021/ja411755t

Hutchings, D.C., Sheik-Bahae, M., Hagan, D.J., et al.: Kramers-Krönig relations in nonlinear optics. Opt Quant Electron **24**, 1–30 (1992). https://doi.org/10.1007/BF01234275

Jayakrishnan, K., Joseph, A., Bhattathiripad, J., Ramesan, M.T., Chandrasekharan, K., Narendran, N.K.S.: Reverse saturable absorption studies in polymerized indole—effect of polymerization in the phenomenal enhancement of third order optical nonlinearity. Opt. Mater. **54**, 252–261 (2016). https://doi.org/10.1016/j.optmat.2016.02.041

Khan, M.U., Ibrahim, M., Khalid, M., Qureshi, M.S., Gulzar, T., Zia, K.M., Al-Saadi, A.A., Janjua, M.R.S.A.: First theoretical probe for efficient enhancement of nonlinear optical properties of quinacridone based compounds through various modifications. Chem. Phys. Lett. **715**, 222–230 (2019). https://doi.org/10.1016/j.cplett.2018.11.051

Khan, M.U., Khalid, M., Khera, R.A., Akhtar, M.N., Abbas, A., Rehman, M.F., Braga, A.A.C., Alam, M.M., Imran, M., Wang, Y., Lu, C.: Influence of acceptor tethering on the performance of nonlinear optical properties for pyrene-based materials with A-π-D-π-D architecture. Arab. J. Chem. **15**(3), 103673 (2022). https://doi.org/10.1016/j.arabjc.2021.103673

Kirtman, B., Luis, J.M., Bishop, D.M.: Simple finite field method for calculation of static and dynamic vibrational hyperpolarizabilities: curvature contributions. J. Chem. Phys. **108**, 10008 (1998). https://doi.org/10.1063/1.476460

Kitamura, M., Arakawa, Y.: Pentacene-based organic field-effect transistors. J. Condens. Matter Phys. **20**, 184011 (2008). https://doi.org/10.1088/0953-8984/20/18/184011

Kymissis, I., Dimitrakopoulos, C.D., Purushothaman, S.: Patterning pentacene organic thin film transistors. J. Vac. Sci. Technol. B Microelectron. Nanometer Struct. Process. Meas. Phenom. **20**, 956 (2002). https://doi.org/10.1116/1.1477427

Lakhera, S., Devlal, K., Ghosh, A., Rana, M.: In silico investigation of phytoconstituents of medicinal herb 'Piper Longum' against SARS-CoV-2 by molecular docking and molecular dynamics analysis. Results Chem. **3**, 100199 (2021). https://doi.org/10.1016/j.rechem.2021.100199

Lakhera, S., Rana, M., Devlal, K., Celik, I., Yadav, R.: A comprehensive exploration of pharmacological properties, bioactivities and inhibitory potentiality of luteolin from Tridax procumbens as anticancer drug by in-silico approach. Struct. Chem. (2022a). https://doi.org/10.1007/s11224-022-01882-7

Lakhera, S., Devlal, K., Ghosh, A., Rana, M.: Modelling the DFT structural and reactivity study of feverfew and evaluation of its potential antiviral activity against COVID-19 using molecular docking and MD simulations. Chem. Pap. **76**, 2759–2776 (2022b). https://doi.org/10.1007/s11696-022-02067-6

Lakhera, S., Rana, M., Devlal, K.: Theoretical study on spectral and optical properties of essential amino acids: a comparative study. Opt Quantum Electron. **54**, 714 (2022c). https://doi.org/10.1007/s11082-022-04118-4

Lakhera, S., Devlal, K., Rana, M., Dhuliya, V.: Quantum mechanical study of three aromatic bioactive fatty alcohol compounds with nonlinear optical and potential light harvesting properties. Opt. Mater. **129**, 112476 (2022d). https://doi.org/10.1016/j.optmat.2022.112476

Lee, J.K., Koo, J.M., Lee, S.Y., Choi, T.Y., Joo, J., Kim, J.Y., Choi, J.H.: Studies of pentacene-based thin film devices produced by cluster beam deposition methods. Opt. Mater. **21**(1–3), 451–454 (2003). https://doi.org/10.1016/S0925-3467(02)00181-7

Li, X., Ma, R., Liu, T., et al.: Fine-tuning HOMO energy levels between PM6 and PBDB-T polymer donors via ternary copolymerization. Sci. China Chem. **63**, 1256–1261 (2020). https://doi.org/10.1007/s11426-020-9805-7

Li, G., Yuan, H., Mou, J., Dai, E., Zhang, H., Li, Z., Zhao, Y., Dai, Y., Zhang, X.: Electrochemical detection of nitrate with carbon nanofibers and copper co-modified carbon fiber electrodes. Compos. Commun. **29**, 101043 (2022). https://doi.org/10.1016/j.coco.2021.101043

Maria, J., Iqbal, K.: Ayub, Enhanced electronic and non-linear optical properties of alkali metal (Li, Na, K) doped boron nitride nano-cages. J. Alloys Compd. (2016b). https://doi.org/10.1016/j.jallcom.2016.06.121

Maria, J., Iqbal, K., Ayub, K.: Enhanced electronic and non-linear optical properties of alkali metal (Li, Na, K) doped boron nitride nano-cages. J. Alloys Compd. **687**, 976–983 (2016). https://doi.org/10.1016/j.jallcom.2016.06.121

Maria, J., Iqbal, Ayub, K.: Theoretical study of the non linear optical properties of alkali metal (Li, Na, K) doped aluminum nitride nanocages. RSC Adv. **6**, 94228–94235 (2016a). https://doi.org/10.1039/C6RA21797D

Maria, J., Iqbal, R., Ludwig, K., Ayub, K.: Phosphides or nitrides for better NLO properties? A detailed comparative study of alkali metal doped nano-cages. Mater. Res. Bull. **92**, 113–122 (2017). https://doi.org/10.1016/j.materresbull.2017.03.065

Mary, Y.S., Bolelli, T.E., Thomas, R., Krishnan, A.R., Bolelli, K., Kasap, E.N., Onkol, T., Yildiz, I.: Quantum mechanical studies of three aromatic halogen-substituted bioactive sulfonamidobenzoxazole compounds with potential light harvesting properties. Polycycl. Aromat. Compd. (2019). https://doi.org/10.1080/10406638.2019.1689405

Mu, S., Liu, Q., Kidkhunthod, P., Zhou, X., Wang, W., Tang, Y.: Molecular grafting towards high-fraction active nanodots implanted in N-doped carbon for sodium dual-ion batteries. Natl. Sci. Rev. **8**(7), 178 (2021). https://doi.org/10.1093/nsr/nwaa178

Munsif, S., Maria, Khan, S., Ali, A., Gilani, M.A., Iqbal, J., Ludwig, R., Ayub, K.: Remarkable nonlinear optical response of alkali metal doped aluminum phosphide and boron phosphide nanoclusters. J. Mol. Liq. **271**, 51–64 (2018). https://doi.org/10.1016/j.molliq.2018.08.121

Ojo, N.D., Krause, R.W., Egbedi, N.O.O.: Electronic and nonlinear optical properties of 2-(((5-aminonaphthalen-1-yl)imino)methyl)phenol: experimental and time-dependent density functional studies. J. Mol. Liq. **319**, 114157 (2020). https://doi.org/10.1016/j.molliq.2020.114157

Omidi, A.R., Dadsetani, M.: Optical properties of phenanthrene: a DFT study for comparison between linear and nonlinear regimes. Solid State Commun. **234–235**, 1–9 (2016). https://doi.org/10.1016/j.ssc.2016.02.018

Otaibi, J.S.A., Mary, Y.S., Mary, Y.S.: Understanding the mechanism of thioguanine's binding to Ag6 and bimetallic (Ag3–Au3 and Ag3–Cu3) clusters. J. Mol. Struct. **1265**, 133415 (2022). https://doi.org/10.1016/j.molstruc.2022.133415

Oyeneyin, O.E., Ojo, N.D., Ipinloju, N., James, A.C., Agbaffa, E.B.: Investigation of corrosion inhibition potentials of some aminopyridine schiff bases using density functional theory and Monte Carlo Simulation. Chem. Afr. **5**, 319–332 (2022). https://doi.org/10.1007/s42250-021-00304-1

Pan, S., Rothberg, L.J.: plasmon enhancement of organic photovoltaic in tandem cells of pentacene/C60. Plasmonics Metallic Nanostruct. Opt. Prop. **6641**, 664109 (2007). https://doi.org/10.1117/12.736011

Poor, P.Z., Flores, J.B.: Theoretical assessment of the selective fluorescence quenching of 1-amino-8-naphthol-3,6-disulfonic acid (H-Acid) complexes with Zn^{2+}, Cd^{2+}, and Hg^{2+}: a DFT and TD-DFT study. J. Phys. Chem. A **118**(51), 12178–12183 (2014). https://doi.org/10.1021/jp511084w

Rana, M., Chowdhury, P.: Effects of hydrogen bonding between pyrrole-2-carboxaldehyde and nearest polar and nonpolar environment. Spectrochim. Acta A Mol. Biomol. **185**, 198–206 (2017). https://doi.org/10.1016/j.saa.2017.05.050

Rana, M., Singla, N., Chatterjee, A., Shukla, A., Chowdhury, P.: Investigation of nonlinear optical (NLO) properties by charge transfer contributions of amine functionalized tetraphenylethylene. Opt. Mater. **62**, 80–89 (2016). https://doi.org/10.1016/j.optmat.2016.09.043

Rana, M., Singla, N., Pathak, A., Dhanya, R., Narayana, C., Chowdhury, P.: Vibrational-electronic properties of intra/inter molecular hydrogen bonded heterocyclic dimer: an experimental and theoretical study of pyrrole-2-carboxaldehyde. Vib. Spectrosc. **89**, 16–25 (2017). https://doi.org/10.1016/j.vibspec.2016.12.003

Rana, M., Chatterjee, A., Chowdhury, P.: Investigation of nonlinear optical properties of organic based di amine substituted tetraphenylethylene. AIP Conf. Proc. **2009**, 020055 (2018). https://doi.org/10.1063/1.5052124

Ruiz, R., Choudhary, D., Nickel, B., Toccoli, T., Chang, K.C., Mayer, A.C., Clancy, P., Blakely, J.M., Headrick, R.L., Iannotta, S., Malliaras, G.G.: Pentacene thin film growth. Chem. Mater. **16**(23), 4497–4508 (2004). https://doi.org/10.1021/cm049563q

Sadowski, J.T.: Pentacene growth on 3-aminopropyltrimethoxysilane modified silicon dioxide. Opt. Mater. **34**(10), 1635–1638 (2012). https://doi.org/10.1016/j.optmat.2012.03.032

Shakerzadeh, E., Mirzavand, H., Mahdavifar, Z.: A comparative DFT study on prospective application of C24, Si12C12, B12N12, B12P12, Al12N12, and Al12P12 nanoclusters as suitable anode materials for magnesium-ion batteries (MIBs). Phys. E Low-Dimens. Syst. Nanostructures **140**, 115161 (2022). https://doi.org/10.1016/j.physe.2022.115161

Srivastava, A., Tripathi, S.: Spectral response optimization in Pentacene and cupric oxide-based photodetector using structural engineering: planar and bulk heterostructure. Opt. Mater. **126**, 112136 (2022). https://doi.org/10.1016/j.optmat.2022.112136

Sun, H.L., Qin, C.S., Qiu, Y.Q., Yang, G.C., Min, Z.: Su, Theoretical investigation of structures, electronic spectra and nonlinear optical properties of gold–pentacene (Au2C22H14) complexes. J. Organomet. Chem. **694**(9–10), 1266–1272 (2009). https://doi.org/10.1016/j.jorganchem.2008.11.053

Tahmasebi, E., Shakerzadeh, E., Biglari, Z.: Theoretical assessment of the electro-optical features of the group III nitrides (B12N12, Al12N12 and Ga12N12) and group IV carbides (C24, Si12C12 and Ge12C12) nanoclusters encapsulated with alkali metals (Li, Na and K). Appl. Surf. Sci. **363**, 197–208 (2016). https://doi.org/10.1016/j.apsusc.2015.12.001

Tekarli, S.M., Drummond, M.L., Williams, T.G., Cundari, T.R., Wilson, A.K.: Performance of density functional theory for 3d transition metal-containing complexes: utilization of the correlation consistent basis sets. J. Phys. Chem. A **113**, 8607–8614 (2009). https://doi.org/10.1021/ct400379z

Tong, X., Zhang, F., Ji, B., Sheng, M., Tang, Y.: Carbon-coated porous aluminum foil anode for high-rate, long-term cycling stability, and high energy density dual-ion batteries. Adv. Mater. **28**(45), 9979–9985 (2016). https://doi.org/10.1002/adma.201603735

Tsague, L.F., Ejuh, G.W., Ndjaka, J.M.B.: Study of the optoelectronic, nonlinear properties and spectroscopic analysis of the molecule fulminene using ab initio and DFT methods. Opt. Quantum Electron. **54**, 621 (2022). https://doi.org/10.1007/s11082-022-03915-1

Weinhold, F., Landis, C.R.: Valency and Bonding. A Natural Bond Orbital Donor-acceptor Perspective. Cambridge University Press, New York (2005)

Wu, Y., Zhao, Y., Han, X., Jiang, G., Shi, J., Liu, P., Khan, M.Z., Huhtinen, H., Zhu, J., Jin, Z., Yamada, Y.: Ultra-fast growth of cuprate superconducting films: dual-phase liquid assisted epitaxy and strong flux pinning. Mater. Today Phys. **18**, 100400 (2021). https://doi.org/10.1016/j.mtphys.2021.100400

Wu, Y., Chen, J., Zhang, L., Ji, J., Wang, Q., Zhang, S.: Effect of boron on the structural stability, mechanical properties, and electronic structures of γ′-Ni3Al in TLP joints of nickel-based single-crystal alloys. Mater. Today Commun. **31**, 103375 (2022). https://doi.org/10.1016/j.mtcomm.2022.103375

Yadav, P., Rana, M., Chowdhury, P.: DFT and MD simulation investigation of favipiravir as an emerging antiviral option against viral protease (3CLpro) of SARS-CoV-2. J. Mol. Struct. **1246**, 131253 (2021). https://doi.org/10.1016/j.molstruc.2021.131253

Yang, G., Fang, L., Tan, K., Shi, S., Su, Z., Wang, R.: Quantum chemical study of structures, electronic spectrum, and nonlinear optical properties of gold−pentacene complexes. Organometallics **26**(8), 2082–2087 (2007). https://doi.org/10.1021/om060955b

Yang, W., Zhang, H., Liu, Y., Tang, C., Xu, X., Liu, J.: Rh(III)-catalyzed synthesis of dibenzo[b, d]pyran-6-ones from aryl ketone O-acetyl oximes and quinones via C-H activation and C–C bond cleavage. RSC Adv. **12**, 14435–14438 (2022). https://doi.org/10.1039/D2RA02074B

Yanxin, Y., Yulin, H., Pan, L., Hui, Z., Qiuying, Z., Jialiang, L., Linghan, X., Xibin, W., Yuhui, A., Ming, L.: Mild and in situ photo-crosslinking of anthracene-functionalized poly(aryl ether ketone) for enhancing temporal stability of organic NLO materials. J Mater Sci **56**, 5910–5923 (2021). https://doi.org/10.1007/s10853-020-05594-3

Yu, S., Wang, X., Ai, Y., Tan, X., Hayat, T., Hu, W., Wang, X.: Experimental and theoretical studies on competitive adsorption of aromatic compounds on reduced graphene oxides. J. Mater. Chem. A **4**, 5654–5662 (2016). https://doi.org/10.1039/C6TA00890A

Zhang, Z., Yang, F., Zhang, H., Zhang, T., Wang, H., Xu, Y., Ma, Q.: Influence of CeO2 addition on forming quality and microstructure of TiCx-reinforced CrTi4-based laser cladding composite coating. Mater. Charact. **171**, 110732 (2021). https://doi.org/10.1016/j.matchar.2020.110732

Zhang, Q., Xin, C., Shen, F., Gong, Y., Zi, Y., Guo, H., Li, Z., Peng, Y., Zhang, Q., Wang, Z.L.: Human body IoT systems based on the triboelectrification effect: energy harvesting, sensing, interfacing and communication. Energy Environ. Sci. **15**, 3688–3721 (2022). https://doi.org/10.1039/D2EE01590K

Zhao, C., Xi, M., Huo, J., He, C.: B-Doped 2D-InSe as a bifunctional catalyst for CO_2/CH_4 separation under the regulation of an external electric field. Phys. Chem. Chem. Phys. **23**, 23219–23224 (2021)

Zhu, H., Zhao, R.: Nucleation of CVD-prepared hexagonal boron nitride on Ni(100), Ni(110) and Ni(111) surfaces: a theoretical study. Vacuum **205**, 111396 (2022). https://doi.org/10.1016/j.vacuum.2022.111396